Received: 20 October 2021 | Revised: 18 January 2022 | Accepted: 20 January 2022

DOI: 10.1002/dvdy.458

Developmental Dynamics WILEY

Embryonic and early postnatal cranial bone volume and tissue mineral density values for C57BL/6J laboratory mice

Kate M. Lesciotto[1] | **Lauren Tomlinson**[2] | **Steven Leonard**[3] | **Joan T. Richtsmeier**[4]

[1]College of Osteopathic Medicine, Sam Houston State University, Conroe, Texas, USA

[2]Department of Biology, New York University, New York, New York, USA

[3]College of Medicine, Drexel University, Philadelphia, Pennsylvania, USA

[4]Department of Anthropology, Pennsylvania State University, University Park, Pennsylvania, USA

Correspondence
Kate M. Lesciotto, Department of Clinical Anatomy, College of Osteopathic Medicine, Sam Houston State University, 925 City Central Avenue, Conroe, TX 77302, USA.
Email: kate.lesciotto@shsu.edu

Joan T. Richtsmeier, Department of Anthropology, Pennsylvania State University, 409 Carpenter Building, University Park, PA 16802, USA.
Email: jta10@psu.edu

Funding information
Eunice Kennedy Shriver National Institute of Child Health and Human Development, Grant/Award Number: P01HD078233; National Institute of Dental and Craniofacial Research, Grant/Award Number: R01DE027677; National Science Foundation, Grant/Award Number: BCS 1731909

Abstract

Background: Laboratory mice are routinely used in craniofacial research based on the relatively close genetic relationship and conservation of developmental pathways between humans and mice. Since genetic perturbations and disease states may have localized effects, data from individual cranial bones are valuable for the interpretation of experimental assays. We employ high-resolution microcomputed tomography to characterize cranial bones of C57BL/6J mice at embryonic day (E) 15.5 and E17.5, day of birth (P0), and postnatal day 7 (P7) and provide estimates of individual bone volume and tissue mineral density (TMD).

Results: Average volume and TMD values are reported for individual bones. Significant differences in volume and TMD during embryonic ages likely reflect early mineralization of cranial neural crest-derived and intramembranously forming bones. Although bones of the face and vault had higher TMD values during embryonic ages, bones of the braincase floor had significantly higher TMD values by P7.

Conclusions: These ontogenetic data on cranial bone volume and TMD serve as a reference standard for future studies using mice bred on a C57BL/6J genetic background. Our findings also highlight the importance of differentiating "control" data from mice that are presented as "unaffected" littermates, particularly when carrying a single copy of a cre-recombinase gene.

KEYWORDS
bone mineralization, bone structure, cranial ossification centers, development

1 | INTRODUCTION

Mice are used routinely in evolutionary and biomedical research, in part based on their relatively close genetic relationship with humans.[1-8] Despite differences in overall cranial proportions and appearance, the deep phylogenetic history between humans and mice is reflected in the conservation of genetic regulatory and developmental

This is an open access article under the terms of the Creative Commons Attribution-NonCommercial-NoDerivs License, which permits use and distribution in any medium, provided the original work is properly cited, the use is non-commercial and no modifications or adaptations are made.
© 2022 The Authors. *Developmental Dynamics* published by Wiley Periodicals LLC on behalf of American Association for Anatomy.

pathways that guide craniofacial growth and development.[2,9-11] Although others exist, the laboratory mouse remains the most widely used vertebrate model organism, particularly for craniofacial research.[1,2,4,10,12-14]

Development of the craniofacial skeleton is complex, with individual bones of the skull having different ontogenetic trajectories and modes of mineralization.[15,16] The creation of transgenic mouse lines to study craniofacial disorders has allowed researchers to study the effects of coding and noncoding genetic variants on skull morphology. However, parsing out the effects of genetic mutations on variation in skull morphology, growth, and development is enhanced by detailed data at the level of the individual cranial bone, based upon differences in the cell population from which each bone is derived (cranial neural crest cells [CNCC] vs mesoderm), mode of ossification (endochondral vs intramembranous), and function as part of a cranial module (facial skeleton vs cranial vault vs braincase floor).[1,2,15-18] While an initial developmental disruption may be directed solely to CNCC-derived elements, once mineralization begins and cranial bones approach each other and cranial soft tissue organs continue to change in size and shape, the local changes to CNCC-derived bones may influence other bones and become more generalized to the skull as a whole.[19,20] The identification of localized patterns of perturbation requires analyses of the formation and growth of individual cranial bones early during the mineralization process and over developmental time.

Bone volume, surface area, cortical thickness, and density are parameters commonly used to quantify the progression of bone growth or as comparative metrics for disease and transgenic mouse models, but the focus is often on the postcranial skeleton.[21-26] Data on prenatal development of individual cranial bones in common laboratory strains of mice are lacking. Even when craniofacial bone data are published, the presentation of the data can complicate comparisons to other studies. For example, some studies report bone volume or surface area only as relative comparisons to littermates (eg, a 10% decrease in bone volume compared to littermates) without providing raw measures.[27,28] In other studies, cranial bones are grouped together as measures of cranial base, calvarial, or total skull volume or density.[17,29-33] Such data do not provide the necessary level of refinement to determine the localized effects of the disease state or genetic perturbation on different modes of ossification, embryonic cell lineages, functions within cranial modules, or any other criterion that could contribute to differential effects across individual cranial elements. Evidence suggests that when differences in global skull growth or morphology are detected, there may be effects on bone mineralization specific to individual cranial bones.[32-34]

Several studies have provided refined data on individual cranial bone development in mice, including estimates of bone volume and density.[27,32,33,35-37] However, these data are only available for newborn or later postnatal mice and are limited to a subset of cranial bones. The embryonic period is a critical phase for the initiation of bone development, with the majority of cranial bones beginning the process of mineralization during embryonic development.[38,39] Along with biomechanical changes, genetic perturbations introduced during embryogenesis have the potential to affect prenatal craniofacial bone development, which may contribute to a postnatal phenotype. Additionally, delays in the onset of bone mineralization or development may only be appreciable during prenatal growth due to subsequent catch-up growth.

Here, we provide estimates of cranial bone volume and tissue mineral density (TMD) for embryonic and early postnatal C57BL/6J mice. C57BL/6J mice were selected based on their widespread usage in the laboratory research. Research has shown that different inbred strains of laboratory mice show differences in bone volume and density measures,[40,41] and C57BL/6J mice are known to have relatively low bone density (https://www.jax.org/strain/000664). Even among C57BL/6 mice, disease phenotypes may vary by specific substrain (eg, C57BL/6J or C57BL/6N), and the choice of substrain should be considered carefully in experimental design.[42]

We employed high-resolution microcomputed tomography (microCT) to characterize bones from the cranial vault, facial skeleton, and braincase floor at embryonic day 15.5 (E15.5), E17.5, day of birth (P0), and postnatal day 7 (P7). These data can serve as a reference standard for future studies that examine craniofacial development, growth, and disease using C57BL/6J mice.

2 | RESULTS

Bone volume and TMD were statistically compared between the male and female samples for each age group for each individual cranial bone. While our sample sizes do not permit significance testing for sex differences in these parameters, there was no evidence in our data to suggest the presence of sexual dimorphism for any element. On the basis of these analyses, we pooled the male and female samples for each group for all further analyses.

2.1 | Analysis of individual bones

As expected, volume of ossified bone increases with age between E15.5 and P7 (Table 1). At E15.5, the number of ossification centers present was highly variable, but all

specimens consistently showed initial mineralization of the maxilla and mandible. There were no significant correlations between either the number of ossification centers or the total volume of bone present and crown-rump length, weight, or developmental age. One E15.5 specimen showed ossification only in the maxilla and mandible, while another E15.5 specimen showed ossification of the maxilla, mandible, premaxilla, palatine, frontal, parietal, squamous temporal, lateral occipital, basioccipital, and zygomatic bones (Figure 1). These data further demonstrate the established variation in developmental stage of embryos, even from the same litter.[43,44]

By E17.5, all specimens showed appreciable ossification for most of the bones considered, with the exception of the ethmoid, nasal, petrous temporal, presphenoid, and squamous occipital, with one specimen additionally lacking ossification of the tympanic ring. At P0, four specimens lacked ossification of the ethmoid, while all other bones had initiated mineralization. Ossification centers for all bones examined in this study were present in all specimens at P7.

The mandible consistently had the highest bone volume across all ages, and the ethmoid and petrous temporal bones experienced rapid growth between P0 and P7 (Figure 2). Most of the measured bones consistently increased in average TMD with age, with several notable exceptions (Table 2; Figure 3). The average TMD of the mandible and maxilla decreased slightly from E17.5 to P0 but then increased from P0 to P7, although the differences in average TMD from E17.5 to P0 were not statistically significant. The palatine, vomer, and zygomatic bones also decreased in average TMD from P0 to P7; however, only the difference in average TMD for the vomer reached statistical significance ($P < .01$).

2.2 | Analysis of tissue origin, ossification process, and cranial module

Bones were grouped according to their tissue origin, ossification process, and cranial module for comparative analyses. Significant differences in bone volume were only present at ages E15.5 and E17.5, with CNCC-derived bones and bones forming via intramembranous ossification having a significantly higher

TABLE 1 Average bone volume (mm^3) for present ossification centers by age

Bone	E15.5	E17.5	P0	P7
Alisphenoid	0	2.17E-03 (1.29E-03)	0.141 (3.20E-02)	0.516 (5.15E-02)
Basioccipital	3.56E-04 (4.38E-04)	2.78E-02 (1.56E-02)	0.419 (6.37E-02)	1.01 (7.38E-02)
Basisphenoid	0	4.08E-03 (5.59E-03)	0.320 (6.29E-02)	1.11 (9.76E-02)
Ethmoid	0	0	2.47E-03 (1.66E-03)	2.01 (0.245)
Frontal	4.36E-03 (2.99E-03)	3.66E-02 (1.31E-02)	0.456 (8.72E-02)	1.70 (0.183)
Interparietal	0	6.11E-04 (5.09E-04)	0.152 (3.18E-02)	1.13 (0.148)
Lateral occipital	5.86E-04 (9.31E-04)	1.44E-02 (1.47E-02)	0.249 (3.50E-02)	0.649 (4.68E-02)
Mandible	1.67E-02 (1.81E-02)	0.115 (3.07E-02)	0.906 (0.223)	3.30 (0.267)
Maxilla	4.38E-03 (3.27E-03)	3.42E-02 (1.12E-02)	0.337 (8.46E-02)	1.72 (0.159)
Nasal	0	0	4.37E-02 (2.24E-02)	0.444 (4.97E-02)
Palatine	9.90E-04 (7.91E-04)	9.32E-03 (3.34E-03)	9.75E-02 (1.71E-02)	0.298 (2.50E-02)
Parietal	1.27E-03 (5.83E-04)	1.00E-02 (5.19E-03)	0.265 (5.12E-02)	1.11 (0.145)
Petrous temporal	0	0	4.66E-02 (3.81E-02)	2.66 (0.500)
Premaxilla	1.05E-03 (8.42E-04)	5.58E-03 (2.53E-03)	0.218 (6.84E-02)	1.18 (0.118)
Presphenoid	0	0	0.122 (3.94E-02)	0.356 (3.22E-02)
Squamous occipital	0	0	0.199 (4.71E-02)	1.05 (0.145)
Squamous temporal	4.55E-04 (2.33E-04)	3.31E-03 (1.33E-03)	0.129 (3.17E-02)	0.715 (7.10E-02)
Tympanic ring	0	3.30E-04 (2.12E-04)	2.23E-02 (4.51E-03)	0.224 (7.01E-02)
Vomer	0	1.52E-03 (1.36E-03)	3.85E-02 (8.74E-03)	0.127 (1.59E-02)
Zygomatic	9.29E-06 (0)	5.83E-04 (3.57E-04)	1.87E-02 (3.48E-03)	9.61E-02 (1.10E-02)

Note: A value of zero indicates that the bone was not present in any specimen at that age. The average standard deviation (SD) of volume for each bone, when present, is indicated in parentheses.

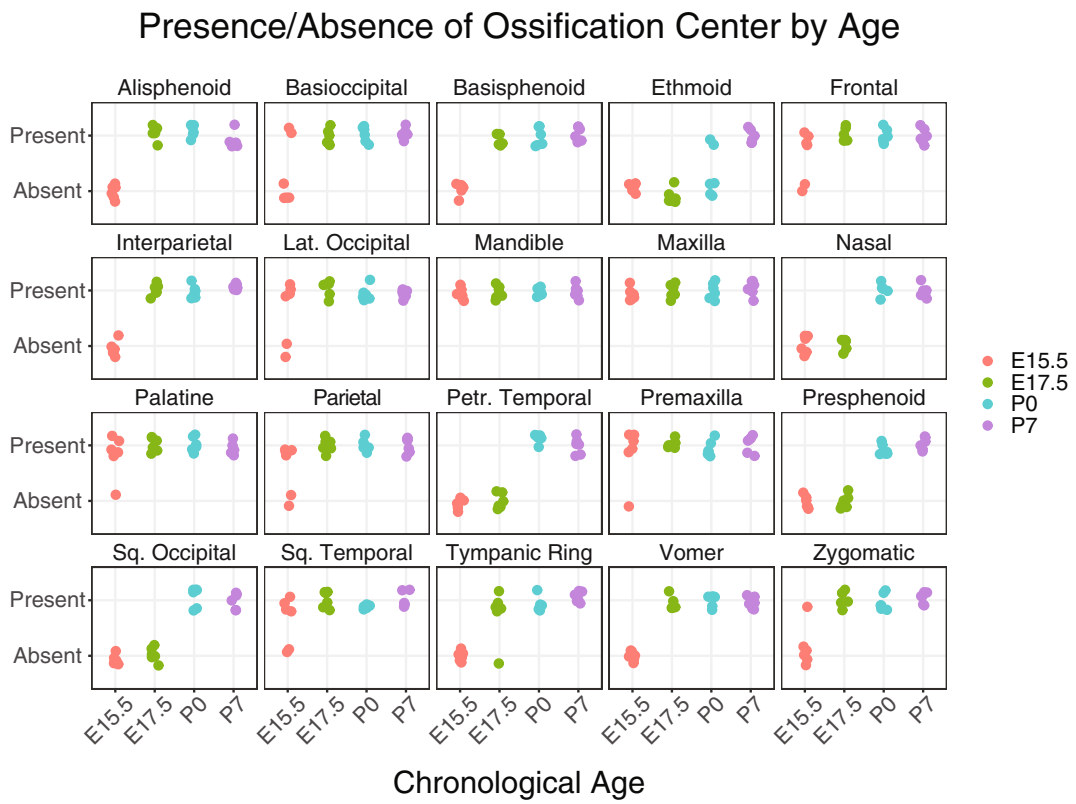

FIGURE 1 Presence/absence of each cranial bone by age. Points are randomly jittered (falsely separated) along the *x*-axis at the represented age group to enable visualization of the value for each specimen, with six individuals represented in each age group

average volume than mesoderm-derived bones and bones forming via endochondral ossification (Figure 4). Additionally, facial bones had a significantly higher average volume than bones of the braincase floor at E15.5. No significant differences in volume were found at P0 or P7, suggesting possible catch-up growth of mesoderm-derived bones, bones forming via endochondral ossification, and bones of the braincase floor or deceleration of growth of the CNCC-derived bones, bones forming via intramembranous ossification, and facial bones.

In contrast, significant differences in average TMD persisted through P7, although the differences detected at P7 show a pattern shift (Figure 5). During embryonic ages, CNCC-derived bones, bones forming via intramembranous ossification, and bones of the vault and face had significantly higher average TMD, while mesoderm-derived bones, bones forming via endochondral ossification, and bones of the braincase floor had significantly higher average TMD at P7. This suggests differential rates of postnatal mineralization within cranial elements grouped by tissue origin, ossification type, and cranial module (eg, through either catch-up or deceleration of growth rates by group).

3 | DISCUSSION

Craniofacial morphological studies of embryonic and early postnatal mice frequently find few or no sex differences and often pool male and female specimens, a finding consistent with our data.[35,36,45,46] The apparent lack of morphological differences between the sexes may be grounded in similarity in embryonic and early postnatal bone development, as no evidence of sexual dimorphism in cranial bone volume or TMD was apparent for any of the examined cranial bones at any of the four ages in this study, but awaits verification with larger sample sizes. Shen et al similarly tested for sex differences at P7 and P21 in volume measurements for six individual cranial bones, finding no significant sexual dimorphism at either age.[32]

Previous studies by Percival and colleagues compared cranial bone volume data between *Fgfr2*$^{+/P253R}$ Apert syndrome mice and unaffected littermates[47] and between *Fgfr2*$^{+/Y394C}$ Beare-Stevenson syndrome mice and unaffected littermates[48] at embryonic and early postnatal ages. As these mice were bred on a C57BL/6J background, they provide a comparable dataset. Comparison of data for the same ages and cranial bones between the

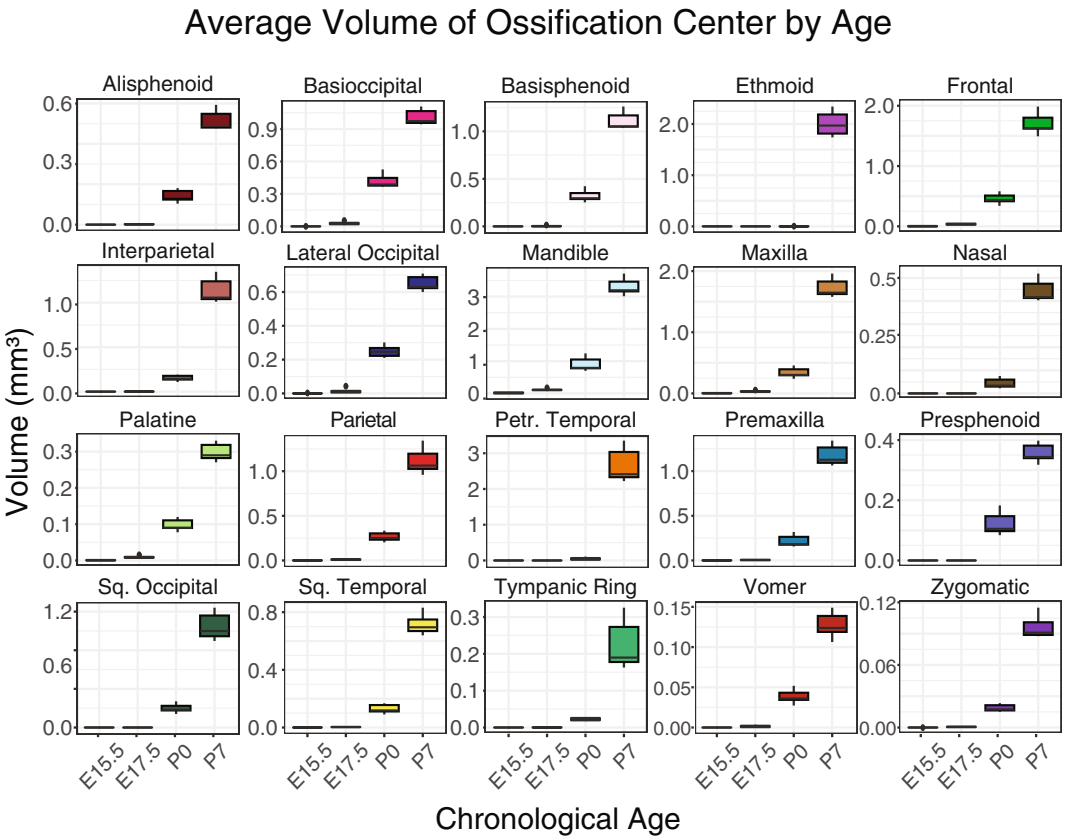

FIGURE 2 Average volume by age for each examined cranial bone. When an ossification center was not present, volume was recorded as 0. *Y*-axis values are separately specified for each bone due to the wide variance in upper values (ranging from 0.12 mm^3 for the zygomatic bone to over 3.5 mm^3 for the mandible)

unaffected littermates of these studies and the C57BL/6J sample analyzed here reveals several differences. Most striking is the observation that mean total cranial bone volume of unaffected littermates of *Fgfr2*$^{+/P253R}$ Apert syndrome mice at E15.5 and E17.5 is more than an order of magnitude greater than the comparable data reported here. This trend continues at P0, with littermates of *Fgfr2*$^{+/P253R}$ Apert syndrome mice reporting mean total bone volumes 25% greater than reported here. The only age group of the unaffected littermates of *Fgfr2*$^{+/Y394C}$ Beare-Stevenson syndrome mice that can be compared to the current study is P0. These data reveal a higher volume for each of the bones measured at P0, excepting the ethmoid, for unaffected littermates of *Fgfr2*$^{+/Y394C}$ Beare-Stevenson syndrome mice relative to data reported here.

These differences in cranial bone volume measures may be due to several differences in methodology. All of the scans used by Percival and colleagues[47,48] were completed using an OMNI-X Universal HD600 microCT system, while the scans used in the present study were conducted with the General Electric v|tom|x L300 nano/microCT system and are characterized by slight differences in voxel sizes. Additionally, semi-automated segmentation methods were used for all postnatal mice in the Percival et al studies,[47,48] while individual cranial bones were manually segmented for mice at all ages in this study. Different minimum thresholds were also used when segmenting ossified bone - 91 mg/cm^3 and 74 mg/cm^3 for the studies by Percival and colleagues, compared with 85 mg/cm^3 for this study.

These differences notwithstanding, a potentially significant consideration is that the study design implemented by Percival and colleagues compared mice carrying a specific disease-associated mutation with littermates that were not affected by the mutation.[47,48] Notably, the unaffected littermates did not carry any floxed genes but were heterozygous for the EIIA-cre recombinase enzyme gene. Unaffected mice that carry a copy of a cre without any floxed genes may still develop unexpected expression patterns and physiological alterations.[49-53] When used as a comparative group for the purpose of defining phenotypic effects of the mutation, these alterations would also occur in the group carrying the mutation, in essence accounting for, or canceling out, these effects and allowing any differences identified between the experimental and comparison groups to be

TABLE 2 Average TMD (mg/cm^3) for present ossification centers by age

Bone	E15.5	E17.5	P0	P7
Alisphenoid	0	192.5 (90.0)	250.9 (37.1)	262.3 (123.3)
Basioccipital	96.9 (11.8)	163.9 (75.2)	301.6 (170.9)	349.3 (165.4)
Basisphenoid	0	140.5 (54.3)	264.7 (134.5)	310.1 (152.8)
Ethmoid	0	0	171.2 (49.3)	233.7 (96.5)
Frontal	121.9 (32.6)	236.3 (119.5)	278.9 (150.1)	292.4 (154.5)
Interparietal	0	112.2 (22.5)	271.3 (136.1)	317.6 (159.4)
Lateral Occipital	104.6 (16.4)	139.2 (60.6)	292.9 (152.3)	328.4 (163.0)
Mandible	118.6 (30.4)	250.7 (136.0)	247.3 (140.8)	321.4 (168.0)
Maxilla	139.9 (43.9)	272.2 (151.3)	257.6 (139.9)	304.4 (160.7)
Nasal	0	0	155.1 (58.1)	233.8 (107.4)
Palatine	118.2 (24.2)	264.4 (137.5)	336.7 (195.1)	307.7 (155.0)
Parietal	113.9 (24.5)	172.9 (71.9)	270.7 (126.2)	303.2 (151.2)
Petrous Temporal	0	0	150.0 (48.6)	292.7 (163.8)
Premaxilla	114.8 (24.3)	206.4 (107.8)	224.3 (114.8)	279.3 (138.1)
Presphenoid	0	0	214.8 (86.9)	278.3 (125.4)
Squamous occipital	0	0	216.4 (89.4)	248.1 (124.0)
Squamous temporal	109.6 (19.1)	206.2 (97.8)	267.6 (147.9)	273.4 (132.2)
Tympanic ring	0	128.0 (28.2)	256.8 (140.0)	387.3 (218.3)
Vomer	0	164.1 (58.2)	316.5 (179.2)	244.7 (120.3)
Zygomatic	90.1 (3.1)	194.1 (81.1)	348.5 (203.1)	308.7 (147.5)

Note: A value of zero indicates that the bone was not present in any specimen at that age. The average SD of TMD values for each bone, when present, is indicated in parentheses.

attributed solely to the introduced mutation. Examination of the Percival et al studies suggests that the cranial bone data for the "wild-type" C57BL/6J mice presented here may not be an appropriate comparative group for other studies that use a cre-recombinase, even if carried on a C57BL/6J background, as those mice may show variation due to the presence of the cre-recombinase gene. Investigators using the cre-lox system should understand that unaffected littermates are not "wild-type" mice and follow recommendations for including a more thorough description of breeding schemes and genotypes for all samples.[52,53]

While there are no additional published TMD data for E15.5-P7 specimens, Wei and colleagues measured bone volume and TMD for small regions of interest in the mandible, frontal, parietal, presphenoid, basisphenoid, and basioccipital bones in P14-P390 C57BL/6NCrl mice.[36] While these data cannot be directly compared to our volume data for the entire bone, comparisons to the observed patterns are useful. At P14, the earliest age measured by Wei et al, the frontal and parietal bones had comparable measures of bone volume and TMD, and both bones followed similar trajectories: a steady increase in volume through P390 and a plateauing of TMD beginning around P30.[36] Our data may provide an extended timeline of TMD for younger mice. The patterns of average TMD for the frontal and parietal bones are similar across the ages studied, with both bones having an average TMD of approximately 300 mg/cm^3 by P7, while Wei et al report a TMD of around 400 mg/cm^3 at P14.[36] Average TMD values for the P7 sample of this study are roughly comparable to the TMD values for the P14 sample of Wei et al for the mandible, presphenoid, basisphenoid, and basioccipital at around 300 mg/cm^3.[36]

Although Percival et al found no significant differences related to tissue origin or ossification type for bone size, density, or rates of bone volume change at P0 or P8,[48] our data support the idea that mesoderm-derived bones exhibit increased bone density compared to CNCC derived bones at early postnatal stages.[34,36,45] Our data showing CNCC derived bones with higher average volume and TMD during prenatal ages may be explained by the observation that the frontal bone, derived from CNCC, begins to mineralize at least 24 hours prior to the parietal bone, which is derived from mesoderm, with other cranial vault bones initializing mineralization even later.[54] Alternatively, the relative lack of mineralized bone prenatally and apparent catch-up seen with postnatal ages may support assertions of delayed initiation or a

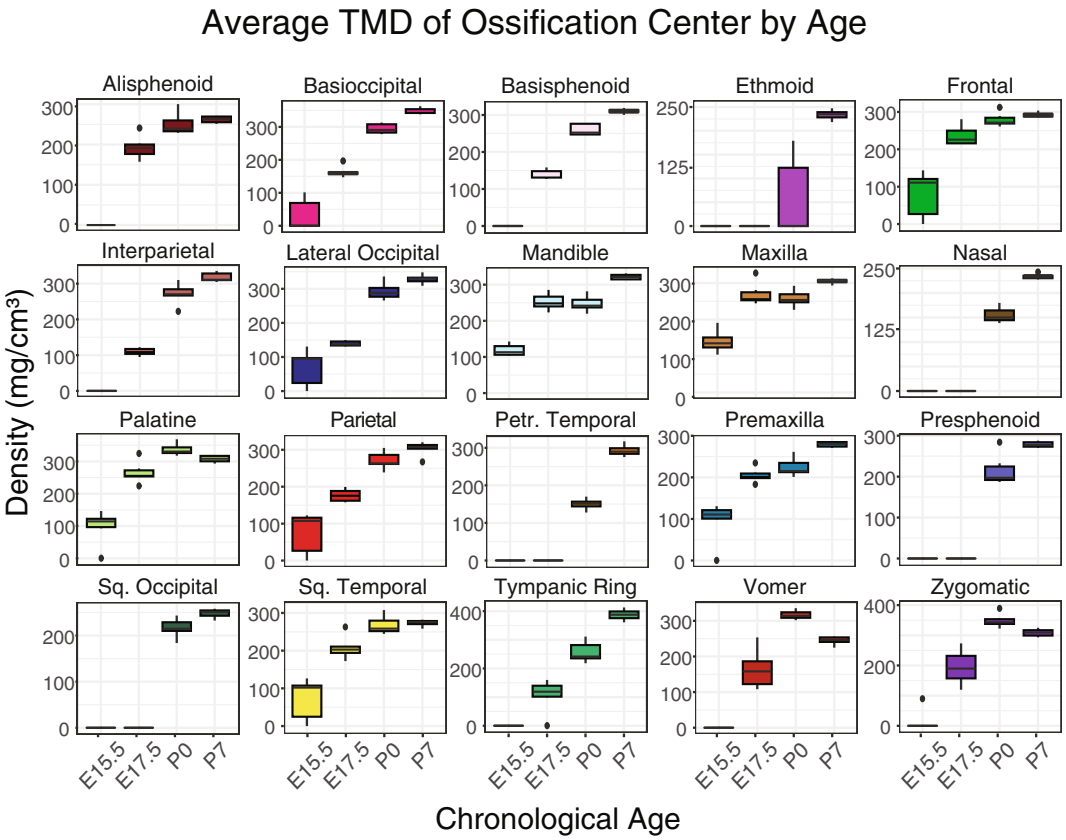

FIGURE 3 Average TMD by age for each examined cranial bone. When an ossification center was not present, TMD was recorded as 0. *Y*-axis values are separately specified for each bone due to the wide variance in upper values (ranging from less than 250 mg/cm^3 for the squamous occipital and nasal bones to over 400 mg/cm^3 for the tympanic ring and zygomatic bones)

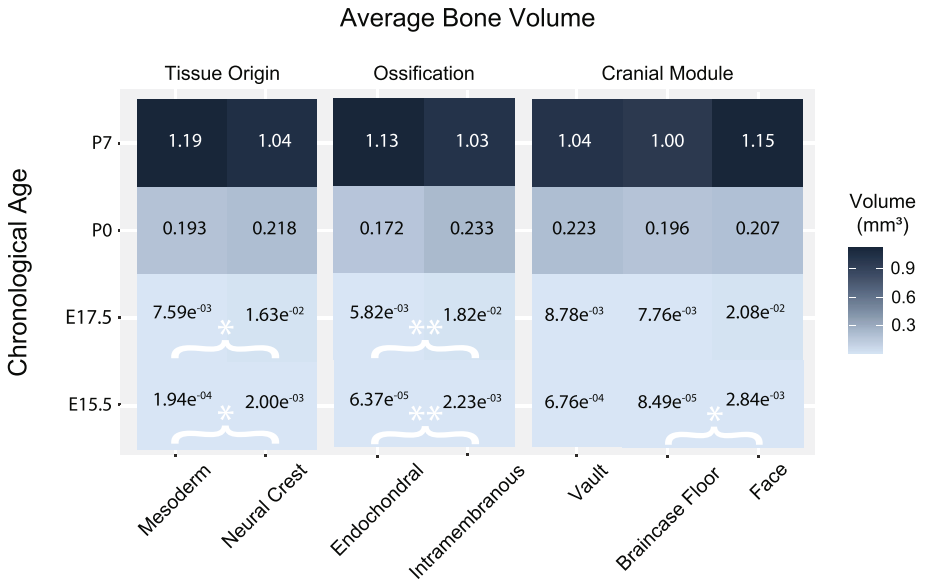

FIGURE 4 Heatmaps of average bone volume across chronological age, with bones grouped by tissue origin (mesoderm v. CNCC), ossification process (endochondral v. intramembranous), and cranial module (face, braincase floor, and vault). *$P < .05$; **$P < .01$

slowed rate of mineralization in mesoderm-derived bones relative to CNCC-derived bones.[55-58]

Pattern shifts in average bone volume and TMD for different cranial regions found by previous research and supported by our data suggest that differences in the functional role of individual cranial bones additionally influences growth and development.[36] The decrease in average TMD between P0 and P7 for the vomer may be the result of rapid antero-posterior growth or may be a reflection of individual differences, as this study is based

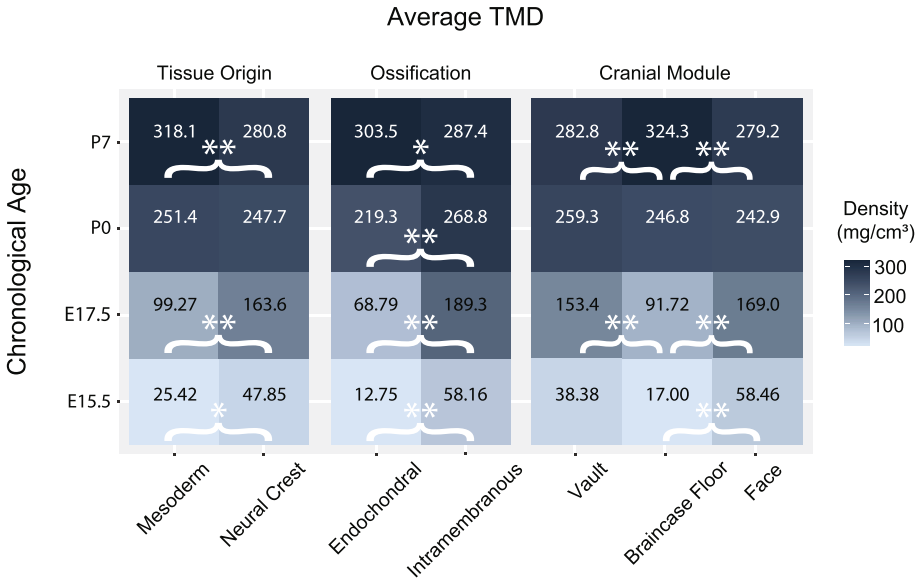

FIGURE 5 Heatmaps of average TMD across chronological age, with bones grouped by tissue origin (mesoderm v. CNCC), ossification process (endochondral v. intramembranous), and cranial module (face, braincase floor, and vault). *$P < .05$; **$P < .01$

TABLE 3 Sample size for each age group

	Age			
	Prenatal		Postnatal	
	E15.5	E17.5	P0	P7
Male	3	3	3	3
Female	3	3	3	3
Total	6	6	6	6

TABLE 4 Average μCT scan settings by age

Age	kV	μA	Average voxel size (mm)
E15.5	100	70	0.006
E17.5	100	60	0.006
P0	100	85	0.009
P7	100	100	0.011

on cross-sectional, rather than longitudinal, data. We also note that average TMD in this study represents the average density of the entire bone and therefore averages the densities between cortical and trabecular bone for each cranial element, leading to questions regarding the differential composition of each element and the coupling of bone resorption and accretion during periods of rapid growth.

Further research is needed, particularly on additional postnatal ages to contextualize bone volume and TMD changes over ontogenetic time, as such data could provide further information about conditions affecting early bone growth and TMD, as well as individual and cooperative contributions to skull morphogenesis.

4 | CONCLUSION

We have established a normative dataset of average volume and TMD for individual cranial bones in C57BL/6J mice from E15.5 through P7. Previous work has demonstrated potentially localized effects of developmental and genetic alterations on individual cranial bones,[32-34] indicating the need for precise, localized data. We note that our data are specific to C57BL/6J mice and the ages studied, as significant differences between adult mice of different inbred strains have been found in postcranial bone parameters.[40,41] Given the heavy usage of C57BL/6J mice, these data may be useful as an established reference standard for average cranial bone volume and TMD in C57BL/6J mice, potentially satisfying the National Institutes of Health requirement for the authentication of key biological resources.

5 | EXPERIMENTAL PROCEDURES

5.1 | Mouse models

All mice used in this study were of the C57BL/6J strain (https://www.jax.org/strain/000664). Based upon timed matings and evidence of pregnancy, litters were sacrificed and collected on E15.5 and E17.5. Postnatal litters were only used if birth occurred on E19 and were collected on the day of birth (P0) and P7. Pregnant dams and postnatal pups were euthanized by inhalation anesthetics. Specimens were fixed in 4% paraformaldehyde in phosphate-buffered saline (PBS). After fixation, the

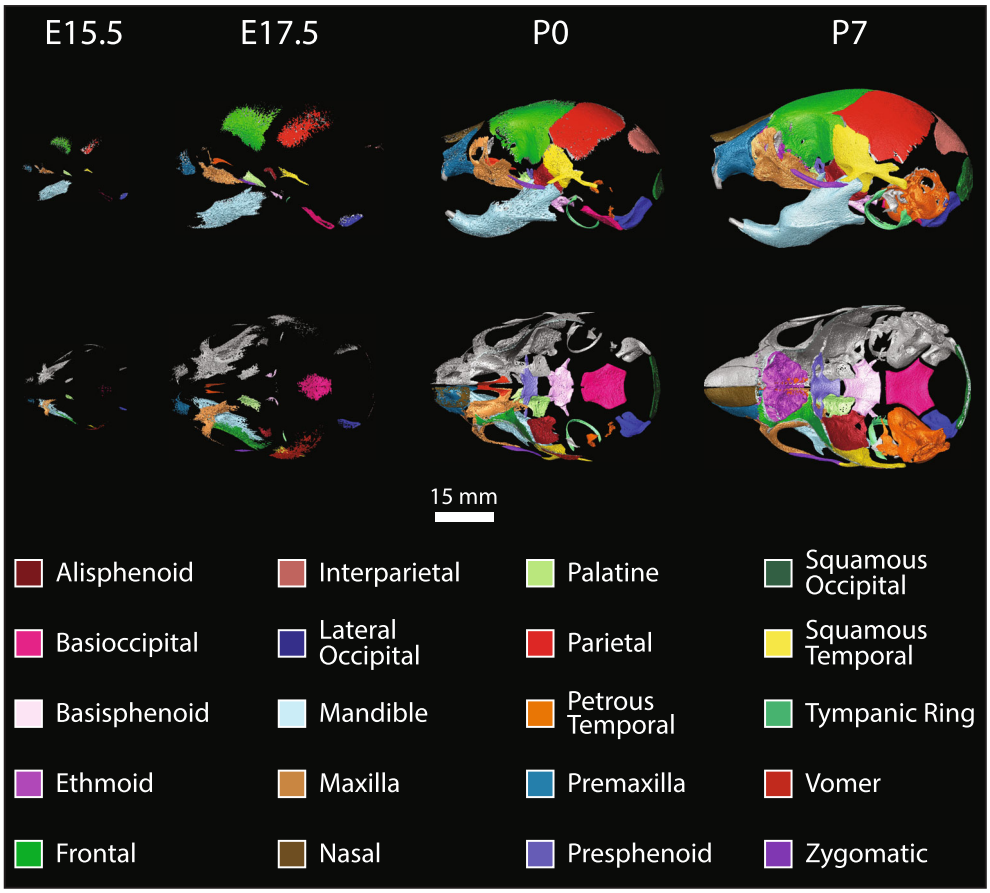

FIGURE 6 Illustration of cranial bones analyzed for this study at each age group. Top row: left lateral view, with the rostrum facing left. Bottom row: superior endocranial view, with the rostrum facing left and the superior portion of the cranial vault removed. Bones that cross the midline were fully segmented. For bilaterally occurring bones, only bones of the left side of the skull were segmented. Bones appearing in gray were not segmented

specimens were disarticulated at the thorax for embryonic samples or the cervical spine for postnatal samples, and the crania were stored in PBS with 0.01% sodium azide as an antibacterial agent until ready for microCT scanning. Sex was confirmed by Y chromosome PCR using a small piece of tail tissue taken at the time of sacrifice. For each age group, the sample represents at least two litters, and individual specimens were selected to represent low, median, and high weights from the available specimens. Relative development of E15.5 specimens was assessed with crown-rump length, weight, and developmental staging using the hind limb according to Musy et al.[44] Sex and age distribution for the sample is described in Table 3. Mice were bred, sacrificed, and processed in compliance with animal welfare guidelines approved by the Pennsylvania State University Animal Care and Use Committee (IACUC # 46558).

5.2 | Image acquisition and data collection

microCT images were acquired by the Center for Quantitative Imaging at the Pennsylvania State University (www.cqi.psu.edu) using the General Electric v|tom|x L300 nano/microCT system. Image data were reconstructed on a 2024 × 2024 pixel grid as a 32-bit volume but were reduced to 16-bit for image analysis with Avizo 9.4 (ThermoFisher). Scanning parameters are provided in Table 4.

Prior to data collection, all postcranial bones were removed from the acquired images using the Volume Edit tool of Avizo 9.4. All scans were then subjected to a 3D median filter to remove background noise. Isosurfaces were reconstructed to represent cranial bone based on a hydroxyapatite phantom that was scanned with each specimen. Scanning the hydroxyapatite phantom with each specimen allowed correlation between X-ray attenuation values and density estimates. The phantom contained five columns of hydroxyapatite in epoxy resin at the following known partial densities: 0, 101.7, 206.2, 403.9, and 792.3 mg/cm^3. Previous morphometric craniofacial studies of embryonic and early prenatal mice have used a minimum threshold of 70-100 mg/cm^3 to create isosurfaces.[47,59,60] To maintain consistency between specimens, 85 mg/cm^3 was used as the minimum threshold to create isosurfaces and segment bone for this study.

Manual, rather than automated, segmentation of individual cranial elements was necessary for embryonic ages due to low levels of ossification, especially for E15.5.

TABLE 5 Cranial bones categorized according to tissue origin, type of ossification process, and cranial module[15]

Bone	Tissue origin	Type of ossification	Cranial module
Alisphenoid	CNCC	Intramembranous	Vault
Basioccipital	Mesoderm	Endochondral	Braincase floor
Basisphenoid	CNCC	Endochondral	Braincase floor
Ethmoid	CNCC	Endochondral	Face
Frontal	CNCC	Intramembranous	Vault
Interparietal	Mixed[a]	Intramembranous	Vault
Lateral occipital	Mesoderm	Endochondral	Braincase floor
Mandible	CNCC	Intramembranous	Face
Maxilla	CNCC	Intramembranous	Face
Nasal	CNCC	Intramembranous	Face
Palatine	CNCC	Intramembranous	Face
Parietal	Mesoderm	Intramembranous	Vault
Petrous temporal	Mesoderm	Endochondral	Braincase floor
Premaxilla	CNCC	Intramembranous	Face
Presphenoid	CNCC	Endochondral	Braincase floor
Squamous occipital	Mesoderm	Endochondral	Vault
Squamous temporal	CNCC	Intramembranous	Vault
Tympanic ring	Mesoderm	Endochondral	Braincase floor
Vomer	CNCC	Intramembranous	Face
Zygomatic	CNCC	Intramembranous	Face

Abbreviation: CNCC, cranial neural crest cells.

[a]The interparietal arises from both mesoderm and CNCC.[61,62] Since the majority originates from mesoderm, the interparietal was grouped with the mesoderm-derived bones for the purposes of all analyses.

Although semi-automated segmentation methods exist for postnatal bone,[47,48] individual cranial bones were also manually segmented in postnatal specimens to ensure accuracy and consistency in methodology across ages groups. Additionally, bridging across sutures between adjacent cranial bones occurred in the P0 and P7 samples (eg, between the frontal and parietal bones), further warranting the more time-consuming manual segmentation methodology, which allowed for visual confirmation that segmentation followed suture morphology and consistency between specimens.

Twenty cranial bones were targeted for individual segmentation for each specimen (Figure 6). Bones that cross the midline (ie, ethmoid, vomer, presphenoid, basisphenoid, basioccipital, squamous occipital, and interparietal) were fully segmented, while only the left side was segmented for bilaterally occurring bones. Volume for each cranial bone was measured using the Material Statistics tool in Avizo 9.4. If a bone that mineralized relatively late in development could not be detected by visualization at an early age, its volume was recorded as 0. TMD was measured by the following three-step process: (a) using ImageJ to derive a regression equation for changing gray values in the scanned image to density values based on the scanned hydroxyapatite phantom with known densities; (2) using this equation to convert pixel gray values to density values; and (3) using the Image Statistics tool in Avizo 9.4 to quantify an average density value for each bone. As this method produced a quantification of the mineral density of ossified tissue only, this parameter is referred to as "tissue mineral density" or TMD. We note that this method takes the average TMD of both cortical and trabecular bone within each cranial element.

Two-sample *t*-tests with Bonferroni correction were used to compare males and females within each age group and to test for significant differences in bone volume and TMD between age groups for the cranial bones examined. T-tests and one-way ANOVAs were performed to test for significant differences in cranial bone volume and TMD based on tissue origin (CNCC v. mesoderm), ossification process (endochondral v. intramembranous), and cranial module (face v. vault v. braincase floor) for each of the examined age groups (Table 5). We note that several cranial bones (eg, mandible, interparietal) either undergo several different types of ossification or have mixed tissue origins; Table 5 reflects the type of ossification or tissue origin that occurs for the majority of the

bone. To evaluate the relative development and variability in ossification center appearance for the E15.5 specimens, Shapiro-Wilk tests were used to determine the normality for the number of ossification centers present, total bone volume, crown-rump length, weight, and developmental age. Pearson correlation tests were used to test for the presence of any significant correlations between either the number of ossification centers present or total volume of bone and crown-rump length, weight, or developmental age.

ACKNOWLEDGMENTS

This work was funded, in part, by the following grants: NIH/NIDCR R01 DE027677, NIH/NICHD P01HD078233, and NSF doctoral dissertation improvement grant BCS-1731909. The authors thank the Center for Quantitative Imaging at the Pennsylvania State University (www.cqi.psu.edu) for their technical assistance and expertise with the General Electric v|tom|x L300 nano/microCT system and Dr. Tim Ryan for his help with developing the protocol for measuring tissue mineral density in Avizo 9.4.

AUTHOR CONTRIBUTIONS

Kate M. Lesciotto: Conceptualization (equal); data curation (lead); formal analysis (equal); funding acquisition (supporting); investigation (equal); methodology (equal); project administration (equal); resources (equal); software (equal); supervision (equal); validation (equal); visualization (equal); writing – original draft (lead); writing – review and editing (equal). **Lauren Tomlinson:** Data curation (supporting); writing – review and editing (supporting). **Steven Leonard:** Data curation (supporting); writing – review and editing (supporting). **Joan T. Richtsmeier:** Conceptualization (equal); data curation (supporting); formal analysis (equal); funding acquisition (lead); investigation (equal); methodology (equal); project administration (equal); resources (equal); software (equal); supervision (equal); validation (equal); visualization (equal); writing – original draft (supporting); writing – review and editing (equal).

ORCID

Kate M. Lesciotto https://orcid.org/0000-0001-9537-5750

Joan T. Richtsmeier https://orcid.org/0000-0002-0239-5822

REFERENCES

1. Lieberman DE, Hallgrímsson B, Liu W, Parsons TE, Jamniczky HA. Spatial packing, cranial base angulation, and craniofacial shape variation in the mammalian skull: testing a new model using mice. *J Anat*. 2008;212(6):720-735. doi:10.1111/j.1469-7580.2008.00900
2. Hallgrímsson B, Lieberman DE. Mouse models and the evolutionary developmental biology of the skull. *Integr Comp Biol*. 2008;48(3):373-384. doi:10.1093/icb/icn076
3. Karpel ME, Boutwell CL, Allen TM. BLT humanized mice as a small animal model of HIV infection. *Curr Opin Virol*. 2015;13:75-80. doi:10.1016/j.coviro.2015.05.002
4. Yang T, Moore M, He F. Pten regulates neural crest proliferation and differentiation during mouse craniofacial development. *Dev Dyn*. 2018;247(2):304-314. doi:10.1002/dvdy.24605
5. Llewellyn GN, Seclén E, Wietgrefe S, et al. Humanized mouse model of HIV-1 latency with enrichment of latent virus in PD-1+ and TIGIT+ CD4 T cells. *J Virol*. 2019;93(10):e02086-e02018. doi:10.1128/JVI.02086-18
6. Yant SR, Mulato A, Hansen D, et al. A highly potent long-acting small-molecule HIV-1 capsid inhibitor with efficacy in a humanized mouse model. *Nat Med*. 2019;25(9):1377-1384. doi:10.1038/s41591-019-0560-x
7. Murphy W, Eizirik E, O'Brien S, et al. Resolution of the early placental mammal radiation using Bayesian phylogenetics. *Science*. 2001;194:2348-2351. doi:10.1126/science.1067179
8. Kriegs JO, Churakov G, Kiefmann M, Jordan U, Brosius J, Schmitz J. Retroposed elements as archives for the evolutionary history of placental mammals. *PLoS Biol*. 2006;4(4):e91. doi:10.1371/journal.pbio.0040091
9. Hallgrímsson B, Willmore K, Dorval C, Cooper DML. Craniofacial variability and modularity in macaques and mice. *J Exp Zoolog B Mol Dev Evol*. 2004;302B(3):207-225. doi:10.1002/jez.b.21002
10. Martínez-Abadías N, Mitteroecker P, Parsons TE, et al. The developmental basis of quantitative craniofacial variation in humans and mice. *Evol Biol*. 2012;39(4):554-567. doi:10.1007/s11692-012-9210-7
11. Perlman RL. Mouse models of human disease: an evolutionary perspective. *Evol Med Public Health*. 2016;2016(1):170-176. doi:10.1093/emph/eow014
12. Motch Perrine SM, Stecko T, Neuberger T, Jabs EW, Ryan TM, Richtsmeier JT. Integration of brain and skull in prenatal mouse models of Apert and Crouzon syndromes. *Front Hum Neurosci*. 2017;11:369. doi:10.3389/fnhum.2017.00369
13. Cibi DM, Mia MM, Shekeran SG, et al. Neural crest-specific deletion of Rbfox2 in mice leads to craniofacial abnormalities including cleft palate. *Elife*. 2019;8:8e45418. doi:10.7554/eLife.45418
14. Richtsmeier JT, Baxter LL, Reeves RH. Parallels of craniofacial maldevelopment in down syndrome and Ts65Dn mice. *Dev Dyn*. 2000;217:137-145. doi:10.1002/(SICI)1097-0177(200002)217:2%3C137::AID-DVDY1%3E3.0.CO;2-N
15. Richtsmeier JT, Flaherty K. Hand in glove: brain and skull in development and dysmorphogenesis. *Acta Neuropathol (Berl)*. 2013;125(4):469-489. doi:10.1007/s00401-013-1104-y
16. Flaherty K, Singh N, Richtsmeier JT. Understanding craniosynostosis as a growth disorder. *WIREs Dev Biol*. 2016;5(4):429-459. doi:10.1002/wdev.227
17. López EKN, Stock SR, Taketo MM, Chenn A, Ravosa MJ. A novel transgenic mouse model of fetal encephalization and craniofacial development. *Integr Comp Biol*. 2008;48(3):360-372. doi:10.1093/icb/icn047
18. López EKN, Stock SR, Taketo MM, Chenn A, Ravosa MJ. MicroCT and microMRI imaging of a prenatal mouse model of

increased brain size. *Proc Int Soc Opt Eng*. 2008;70781T:0781T-1–7-781T-12. doi:10.1117/12.793842

19. Holmes G, Basilico C. Mesodermal expression of *Fgfr2*^{S252W} is necessary and sufficient to induce craniosynostosis in a mouse model of Apert syndrome. *Dev Biol*. 2012;368(2):283-293. doi:10.1016/j.ydbio.2012.05.026
20. Heuzé Y, Singh N, Basilico C, Jabs EW, Holmes G, Richtsmeier JT. Morphological comparison of the craniofacial phenotypes of mouse models expressing the Apert FGFR2 S252W mutation in neural crest- or mesoderm-derived tissues. *Bone*. 2014;63:101-109. doi:10.1016/j.bone.2014.03.003
21. Filvaroff EH, Guillet S, Zlot C, et al. Stanniocalcin 1 alters muscle and bone structure and function in transgenic mice. *Endocrinology*. 2002;143(9):3681-3690. doi:10.1210/en.2001-211424
22. Wang Y, Wan C, Deng L, et al. The hypoxia-inducible factor α pathway couples angiogenesis to osteogenesis during skeletal development. *J Clin Invest*. 2007;117(6):1616-1626. doi:10.1172/JCI31581
23. Liang C, Oest ME, Jones JC, Prater MR. Gestational high saturated fat diet alters C57BL/6 mouse perinatal skeletal formation. *Birth Defects Res B Dev Reprod Toxicol*. 2009;86(5):362-369. doi:10.1002/bdrb.20204
24. Luo J, Zhou W, Zhou X, et al. Regulation of bone formation and remodeling by G-protein-coupled receptor 48. *Development*. 2009;136(16):2747-2756. doi:10.1242/dev.033571
25. Powell WF, Barry KJ, Tulum I, et al. Targeted ablation of the PTH/PTHrP receptor in osteocytes impairs bone structure and homeostatic calcemic responses. *J Endocrinol*. 2011;209(1):21-32. doi:10.1530/JOE-10-0308
26. Davey RA, Clarke MV, Sastra S, et al. Decreased body weight in young Osterix-Cre transgenic mice results in delayed cortical bone expansion and accrual. *Transgenic Res*. 2012;21(4):885-893. doi:10.1007/s11248-011-9581-z
27. Ho TV, Iwata J, Ho HA, et al. Integration of comprehensive 3D microCT and signaling analysis reveals differential regulatory mechanisms of craniofacial bone development. *Dev Biol*. 2015;400(2):180-190. doi:10.1016/j.ydbio.2015.02.010
28. Gou Y, Li J, Wu J, et al. Prmt1 regulates craniofacial bone formation upstream of Msx1. *Mech Dev*. 2018;152:13-20. doi:10.1016/j.mod.2018.05.001
29. Kawaguchi J, Azuma Y, Hoshi K, et al. Targeted disruption of cadherin-11 leads to a reduction in bone density in calvaria and long bone metaphyses. *J Bone Miner Res*. 2001;16(7):1265-1271. doi:10.1359/jbmr.2001.16.7.1265
30. Deckelbaum RA, Majithia A, Booker T, Henderson JE, Loomis CA. The homeoprotein engrailed 1 has pleiotropic functions in calvarial intramembranous bone formation and remodeling. *Development*. 2006;133(1):63-74. doi:10.1242/dev.02171
31. Benson MD, Opperman LA, Westerlund J, et al. Ephrin-B stimulation of calvarial bone formation. *Dev Dyn*. 2012;241(12):1901-1910. doi:10.1002/dvdy.23874
32. Shen L, Ai H, Liang Y, et al. Effect of prenatal alcohol exposure on bony craniofacial development: a mouse MicroCT study. *Alcohol*. 2013;47(5):405-415. doi:10.1016/j.alcohol.2013.04.005
33. Liu J, Nam HK, Campbell C, da Silva Gasque KC, Millán JL, Hatch NE. Tissue-nonspecific alkaline phosphatase deficiency causes abnormal craniofacial bone development in the *Alpl*$^{-/-}$ mouse model of infantile hypophosphatasia. *Bone*. 2014;67:81-94. doi:10.1016/j.bone.2014.06.040
34. Liu J, Campbell C, Nam HK, et al. Enzyme replacement for craniofacial skeletal defects and craniosynostosis in murine hypophosphatasia. *Bone*. 2015;78:203-211. doi:10.1016/j.bone.2015.05.005
35. Vora SR, Camci ED, Cox TC. Postnatal ontogeny of the cranial base and craniofacial skeleton in male C57BL/6J mice: a reference standard for quantitative analysis. *Front Physiol*. 2016;6:1-14. doi:10.3389/fphys.2015.00417
36. Wei X, Thomas N, Hatch NE, Hu M, Liu F. Postnatal craniofacial skeletal development of female C57BL/6NCrl mice. *Front Physiol*. 2017;8:1-18. doi:10.3389/fphys.2017.00697
37. Thompson J, Mendoza F, Tan E, et al. A cleft lip and palate gene, *Irf6*, is involved in osteoblast differentiation of craniofacial bone. *Dev Dyn*. 2019;248(3):221-232. doi:10.1002/dvdy.13
38. Long F. Building strong bones: molecular regulation of the osteoblast lineage. *Nat Rev Mol Cell Biol*. 2012;13(1):27-38. doi:10.1038/nrm3254
39. Kawasaki K, Richtsmeier JT. Association of the chondrocranium and dermatocranium in early skull formation. In: Percival CJ, Richtsmeier JT, eds. *Building Bones: Bone Formation and Development in Anthropology*. Cambridge, United Kingdom: Cambridge University Press; 2017:52-78.
40. Beamer WG, Donahue LR, Rosen CJ, Baylink DJ. Genetic variability in adult bone density among inbred strains of mice. *Bone*. 1996;18(5):397-403. doi:10.1016/8756-3282(96)00047-6
41. Sheng MH-C, Baylink DJ, Beamer WG, et al. Histomorphometric studies show that bone formation and bone mineral apposition rates are greater in C3H/HeJ (high-density) than C57BL/6J (low-density) mice during growth. *Bone*. 1999;25(4):421-429. doi:10.1016/S8756-.3282(99)00184-2
42. Kang SK, Hawkins NA, Kearney JA. C57BL/6J and C57BL/6N substrains differentially influence phenotype severity in the *Scn1a*$^{+/-}$ mouse model of Dravet syndrome. *Epilepsia Open*. 2018;4(1):164-169. doi:10.1002/epi4.12287
43. Flaherty K, Richtsmeier J. It's about time: ossification center formation in C57BL/6 mice from E12–E16. *J Dev Biol*. 2018;6(4):31.
44. Musy M, Flaherty K, Raspopovic J, Robert-Moreno A, Richtsmeier JT, Sharpe J. A quantitative method for staging mouse embryos based on limb morphometry. *Development*. 2018;145(7):dev154856. doi:10.1242/dev.154856
45. Liu J, Nam HK, Wang E, Hatch NE. Further analysis of the Crouzon mouse: effects of the FGFR2 C342Y mutation are cranial bone–dependent. *Calcif Tissue Int*. 2013;92(5):451-466. doi:10.1007/s00223-013-9701-2
46. Motch Perrine SM, Wu M, Stephens NB, et al. Mandibular dysmorphology due to abnormal embryonic osteogenesis in FGFR2-related craniosynostosis mice. *Dis Model Mech*. 2019;12(5):mm038513. doi:10.1242/dmm.038513
47. Percival CJ, Huang Y, Jabs EW, Li R, Richtsmeier JT. Embryonic craniofacial bone volume and bone mineral density in *Fgfr2*$^{+/P253R}$ and nonmutant mice. *Dev Dyn*. 2014;243(4):541-551. doi:10.1002/dvdy.24095
48. Percival CJ, Wang Y, Zhou X, Jabs EW, Richtsmeier JT. The effect of a Beare-Stevenson syndrome *Fgfr2* Y394C mutation on early craniofacial bone volume and relative bone mineral

density in mice. *J Anat*. 2012;221(5):434-442. doi:10.1111/j.1469-7580.2012.01555

49. Matthaei KI. Genetically manipulated mice: a powerful tool with unsuspected caveats. *J Physiol*. 2007;582(2):481-488. doi:10.1113/jphysiol.2007.134908
50. Jeannotte L, Aubin J, Bourque S, Lemieux M, Montaron S, Provencher S-PA. Unsuspected effects of a lung-specific cre deleter mouse line. *Genesis*. 2011;49(3):152-159. doi:10.1002/dvg.20720
51. Harno E, Cottrell EC, White A. Metabolic pitfalls of CNS cre-based technology. *Cell Metab*. 2013;18(1):21-28. doi:10.1016/j.cmet.2013.05.019
52. Dorà NJ, Collinson JM, Hill RE, West JD. Hemizygous Le-Cre transgenic mice have severe eye abnormalities on some genetic backgrounds in the absence of loxP sites. *PLoS ONE*. 2014;9(10):e109193. doi:10.1371/journal.pone.0109193
53. Song AJ, Palmiter RD. Detecting and avoiding problems when using the Cre–lox system. *Trends Genet*. 2018;34(5):333-340. doi:10.1016/j.tig.2017.12.008
54. Pitirri MK, Kawasaki K, Richtsmeier JT. It takes two: building the vertebrate skull from chondrocranium and dermatocranium. *Vertebr Zool*. 2020;70(4):587-600.
55. Quarto N, Wan DC, Kwan MD, Panetta NJ, Li S, Longaker MT. Origin matters: differences in embryonic tissue origin and Wnt signaling determine the osteogenic potential and healing capacity of frontal and parietal calvarial bones. *J Bone Miner Res*. 2009;091123192917092-42:1680-1694. doi:10.1359/jbmr.091116
56. Quarto N, Behr B, Li S, Longaker MT. Differential FGF ligands and FGF receptors expression pattern in frontal and parietal calvarial bones. *Cells Tissues Organs*. 2009;190(3):158-169. doi:10.1159/000202789
57. Li S, Quarto N, Longaker MT. Activation of FGF signaling mediates proliferative and osteogenic differences between neural crest derived frontal and mesoderm parietal derived bone. *PLoS ONE*. 2010;5(11):e14033. doi:10.1371/journal.pone.0014033
58. Li S, Meyer NP, Quarto N, Longaker MT. Integration of multiple signaling regulates through apoptosis the differential osteogenic potential of neural crest-derived and mesoderm-derived osteoblasts. *PLoS ONE*. 2013;8(3):e58610. doi:10.1371/journal.pone.0058610
59. Martínez-Abadías N, Heuzé Y, Wang Y, Jabs EW, Aldridge K, Richtsmeier JT. FGF/FGFR signaling coordinates skull development by modulating magnitude of morphological integration: evidence from Apert syndrome mouse models. *PLoS ONE*. 2011;6(10):e26425. doi:10.1371/journal.pone.0026425
60. Motch Perrine SM, Cole TM, Martínez-Abadías N, Aldridge K, Jabs EW, Richtsmeier JT. Craniofacial divergence by distinct prenatal growth patterns in Fgfr2 mutant mice. *BMC Dev Biol*. 2014;14(1):1-17. doi:10.1186/1471-213X-14-8
61. Gross JB, Hanken J. Review of fate-mapping studies of osteogenic cranial neural crest in vertebrates. *Dev Biol*. 2008;317(2):389-100. doi:10.1016/j.ydbio.2008.02.046
62. Jiang X, Iseki S, Maxon RE, Sucov HM, Morriss-Kay GM. Tissue origins and interactions in the mammalian skull vault. *Dev Biol*. 2002;241(1):106-116. doi:10.1006/dbio.2001.0487

How to cite this article: Lesciotto KM, Tomlinson L, Leonard S, Richtsmeier JT. Embryonic and early postnatal cranial bone volume and tissue mineral density values for C57BL/6J laboratory mice. *Developmental Dynamics*. 2022;251(7):1196-1208. doi:10.1002/dvdy.458